THE ASTROPHYSICAL JOURNAL, 415:505–516, 1993 October 1

POLARIZATION CHANGES OF RADIATION THROUGH STIMULATED RAMAN SCATTERING

R. T. GANGADHARA[1] AND V. KRISHAN
Indian Institute of Astrophysics, Bangalore–560 034, India
Received 1993 January 12; accepted 1993 April 8

ABSTRACT

We study change in the polarization of electromagnetic waves due to the stimulated Raman scattering in a plasma. In this process an electromagnetic wave undergoes coherent scattering off an electron plasma wave. It is found that some of the observed polarization properties such as the rapid temporal variations, sense reversal, rotation of the plane of polarization, and change of nature of polarization in the case of pulsars and quasars could be accounted for through stimulated Raman scattering.

Subject headings: galaxies: active — plasmas — polarization — pulsars: general — radiation mechanism: miscellaneous

1. INTRODUCTION

By assuming a synchrotron origin for the radiation in compact extragalactic radio sources, source models are readily constructed which explain both the spectral and temporal behavior of intensity (e.g., van der Laan 1966; Blandford & Königl 1979), but polarization does not lend itself to such a straightforward explanation. The problems arise mainly from the observed ratio of circular to linear polarization; also, depolarization by a factor of 10 or more is often observed. It is important to determine whether this depolarization is a geometric effect or results from radiation-plasma interactions. There have been only very preliminary attempts to explain depolarization and microvariability using plasma mechanisms.

The change in polarization of an electromagnetic (EM) wave due to its propagation in a magnetized plasma as well as due to an electron scattering is well known. In a magnetized plasma, the Faraday rotation is recognized to be the most common cause of the rotation of the plane of polarization of an EM wave. In a plasma, the spectral components of radiation of finite bandwidth travel different path lengths. This may lead to depolarization. Any change in the direction of the magnetic field also manifests itself through polarization variation. The strong linear polarization observed in the radio as well as in the optical regions of the spectrum in the BL Lacertae objects is believed to originate in the source itself. The fact that optically violently variables and NGC 1275 show similar polarization characteristics, suggests that BL Lac objects, quasars, and Seyfert galaxies have a similar source of energy. If so, then the lack of polarization in quasars and Seyfert galaxies could be due to depolarization effects (Stockman 1978). The rotation of the electric vector has been observed in core-jet structure of 3C 454.3 (Cotton et al. 1984) and is interpreted to be due to the propagation of radiation in a medium of varying optical thickness.

A powerful collective emission occurs when relativistic electron beams with density exceed 1% of the background plasma density scatter off coherently from concentrations of electrostatic plasma waves (cavitons) (Benford 1992). The polarization of the emitted radiation depends on the orientation and shape of cavitons. Assuming the usual power-law spectrum for electron energies, polarization features mimic synchrotron radiation (Baker et al. 1988; Weatherall & Benford 1991).

In pulsars, the ambient magnetic field determines the orientation of the polarization ellipse, but with an ambiguity of $\pi/2$: the instantaneous angle often attains bimodal distribution with modes separated by $\sim\pi/2$. The relative frequency of occurrence of the modes is a strong function of both pulse longitude and pulsar. The modes are actually elliptically polarized such that one angle correlates with one sense of circular polarization and the orthogonal angle correlates with the other sense. Several pulsars exhibit one or more reversals of the sense of polarization through the profile. The appearance of strong circular polarization (sometimes $>50\%$) implies conversion of the elliptically produced radiation somewhere along the propagation path. Apart from the appearance of circular polarization, however, pulsar magnetospheres do not appear to be magnetoactive (no generalized Faraday rotation is evident) (Cordes 1983). For pulsars in which the integrated profile is highly polarized, essentially all subpulses, must likewise be highly polarized and have stable polarization characteristics. However, many pulsars have rather weakly polarized integrated profiles. Three possible reasons for low polarization, apart from the Faraday rotation, electron scattering, and magnetic field orientations, are that (Manchester & Taylor 1977) the subpulses at a given longitude may (1) be themselves weakly polarized, (2) be divisible into groups with orthogonal polarization, or (3) have randomly varying position angles and sense of circular polarization.

Collective plasma processes have been shown to play significant roles in the absorption and spectral modification of the radiation through its interaction with the plasma in the accretion disk and the emission-line regions (Beal 1990; Krishan & Wiita 1990; Benford 1992; Gangadhara & Krishan 1990, 1992; Krishan & Gangadhara 1992). This paper shows that in strong radio sources, the rapid temporal variations, sense reversal of rotation of electric field, rotation of plane of polarization, and change of nature of polarization in the case of quasars and pulsars may be accounted for through stimulated Raman scattering (SRS). In this process, an intense EM wave scatters off an electron plasma wave resulting in the scattered EM wave. The physics of SRS in a plasma has been explained in many papers and books (e.g., Drake et al. 1974; Liu & Kaw 1976; Hasegawa 1978; Kruer 1988). The role of stimulated Compton and Raman scattering in the quasar continuum has been shown by Gangadhara & Krishan (1992). Polarization changes through SRS may take place in accretion disks, the emission-line regions, and the intercloud medium of active galactic nuclei and

[1] Also Joint Astronomy Program, Department of Physics, Indian Institute of Science, Bangalore. Electronic mail: ganga@iiap.ernet.in.

also in the emission region of pulsars. In § 2, we derive the dispersion relation describing the SRS of an EM wave. In § 3, to describe the polarization states of the incident and the scattered EM waves, we define Stokes parameters. In § 4, we numerically solve the dispersion relation to find the value of the growth rate of the SRS instability (see Fig. 2). In § 5, we make a comparison between SRS and the well-known process of the Faraday rotation. We investigate the condition under which (e.g., in Fig. 5, growth rate $\Gamma \approx 10^{-5}$ s^{-1}) SRS dominates over the Faraday rotation. The effect of incoherence in the EM waves on SRS instability is discussed in § 6.

2. STIMULATED RAMAN SCATTERING

We begin with a model consisting of a pulsar with nonthermal component of radiation interacting with the plasma in the emission region at a distance $r = 100\,R_{NS} = 10^8$ cm (neutron star radius $R_{NS} \approx 10$ km). In the case of a quasar, we consider a black hole surrounded by a plasma which extends to a few parsecs. The nonthermal continuum is considered as a pump which drives SRS. Here, we consider an electron-ion plasma with uniform and isotropic distribution of temperature and density and assume that it is at rest with respect to the source of radiation.

Consider a large-amplitude elliptically polarized EM wave,

$$\boldsymbol{E}_i = \epsilon_i[\cos(\boldsymbol{k}_i \cdot \boldsymbol{r} - \omega_i t)\hat{e}_1 + \alpha_i \cos(\boldsymbol{k}_i \cdot \boldsymbol{r} - \omega_i t + \delta_i)\hat{e}_2] , \tag{1}$$

propagating in a plasma with density n_0 and temperature T_e.

We can think of $\boldsymbol{E}_i$ as the superposition of two linearly polarized waves: $\boldsymbol{E}_{i1} = \epsilon_i \cos(\boldsymbol{k}_i \cdot \boldsymbol{r} - \omega_i t)\hat{e}_1$ and $\boldsymbol{E}_{i2} = \alpha_i \epsilon_i \cos(\boldsymbol{k}_i \cdot \boldsymbol{r} - \omega_i t + \delta_i)\hat{e}_2$. Let

$$\delta n_{e1} = \delta n_1 \cos(\boldsymbol{k} \cdot \boldsymbol{r} - \omega t) \tag{2}$$

and

$$\delta n_{e2} = \delta n_2 \cos(\boldsymbol{k} \cdot \boldsymbol{r} - \omega t + \delta_e) \tag{3}$$

be the density perturbations in a plasma with equilibrium density n_0. Assume that δn_{e1} couples with $\boldsymbol{E}_{i1}$ and δn_{e2} couples with $\boldsymbol{E}_{i2}$. The coupling between the radiation and the density perturbations is nonlinear because of the ponderomotive force ($\propto \nabla E_{i1}^2$ and $\propto \nabla E_{i2}^2$). Consequently, density perturbations grow up and lead to currents at $(\boldsymbol{k}_i \pm \boldsymbol{k}, \omega_i \pm \omega)$. These currents will generate mixed electromagnetic-electrostatic sideband modes at $(\boldsymbol{k}_i \pm \boldsymbol{k}, \omega_i \pm \omega)$. The sideband modes, in turn, interact with the incident wave field producing a ponderomotive force which amplifies the original density perturbation. Thus, there is a positive feedback system which leads to an instability.

The electric field $\boldsymbol{E}_s$ of the EM wave scattered through an angle ϕ_s with respect to $\boldsymbol{k}_i$ can be written as

$$\boldsymbol{E}_s = \epsilon_s[\cos(\boldsymbol{k}_s \cdot \boldsymbol{r} - \omega_s t)\hat{e}'_1 + \alpha_s \cos(\boldsymbol{k}_s \cdot \boldsymbol{r} - \omega_s t + \delta_s)\hat{e}'_2] . \tag{4}$$

Figure 1 shows the directions of $\boldsymbol{k}_i$ and $\boldsymbol{k}_s$ in the orthogonal coordinate systems $(\hat{e}_1, \hat{e}_2, \hat{e}_3)$ and $(\hat{e}'_1, \hat{e}'_2, \hat{e}'_3)$. The coordinate system $(\hat{e}'_1, \hat{e}'_2, \hat{e}'_3)$ is rotated through an angle ϕ_s about an axis parallel to $\hat{e}_2$. Here, $\boldsymbol{k}_i \parallel \hat{e}_3$, $\boldsymbol{k}_s \parallel \hat{e}'_3$ and $\hat{e}'_2 \parallel \hat{e}_2$. The unit vectors are related by

$$\hat{e}'_1 = \cos(\phi_s)\hat{e}_1 - \sin(\phi_s)\hat{e}_3 , \qquad \hat{e}'_2 = \hat{e}_2 , \qquad \hat{e}'_3 = \sin(\phi_s)\hat{e}_1 + \cos(\phi_s)\hat{e}_3 . \tag{5}$$

The scattered wave in the coordinate system $(\hat{e}_1, \hat{e}_2, \hat{e}_3)$ is given by

$$\boldsymbol{E}_s = \epsilon_s\{\cos(\boldsymbol{k}_s \cdot \boldsymbol{r} - \omega_s t)[\cos(\phi_s)\hat{e}_1 - \sin(\phi_s)\hat{e}_3] + \alpha_s \cos(\boldsymbol{k}_s \cdot \boldsymbol{r} - \omega_s t + \delta_s)\hat{e}_2\} . \tag{6}$$

The wave equation for the scattered the EM wave is given by

$$\left(\nabla^2 - \frac{1}{c^2}\frac{\partial^2}{\partial t^2}\right)\boldsymbol{E}_s = \frac{4\pi}{c^2}\frac{\partial \boldsymbol{J}}{\partial t} , \tag{7}$$

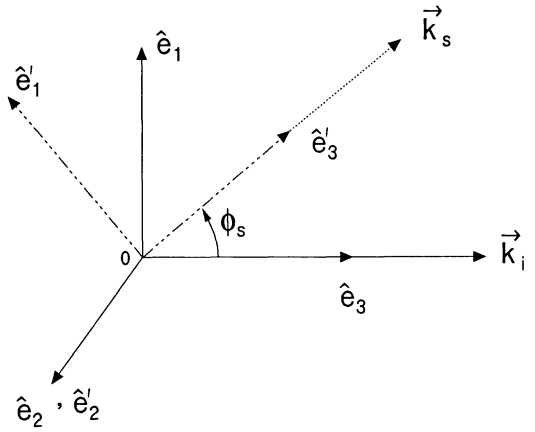

FIG. 1.—The wavevectors and the electric fields of the incident and the scattered EM waves

where c is the velocity of light and $\boldsymbol{J}$ is the current density. The components of the current density are $J_1 = -en_{e1}u_{e1} = -e(n_0 + \delta n_{e1})u_{e1}$, $J_2 = -en_{e2}u_{e2} = -e(n_0 + \delta n_{e2})u_{e2}$ and $J_3 = -en_0 u_{e3}$, where u_{e1}, u_{e2}, and u_{e3} are the components of the oscillation velocity $\boldsymbol{u}_e$ of electrons in the radiation fields $\boldsymbol{E}_i$ and $\boldsymbol{E}_s$. We obtain $\boldsymbol{u}_e$ from the equation

$$\frac{\partial \boldsymbol{u}_e}{\partial t} = -\frac{e}{m_0}(\boldsymbol{E}_i + \boldsymbol{E}_s)\,, \tag{8}$$

where e and m_0 are the charge and the rest mass of an electron.

In SRS, the scattered radiation consists of the Stokes mode $(\boldsymbol{k}_-, \omega_-)$ and the anti-Stokes mode $(\boldsymbol{k}_+, \omega_+)$ with electric fields

$$\boldsymbol{E}_\pm = \epsilon_\pm\{\cos(\boldsymbol{k}_\pm \cdot \boldsymbol{r} - \omega_\pm t)[\cos(\phi_\pm)\hat{e}_1 - \sin(\phi_\pm)\hat{e}_3] + \alpha_\pm \cos(\boldsymbol{k}_\pm \cdot \boldsymbol{r} - \omega_\pm t + \delta_-)\hat{e}_2\}\,. \tag{9}$$

Now, separating the components of equation (7), we have

$$D_\pm E_{\pm 1} = -\frac{2\pi e^2}{m_0}\epsilon_i \delta n_1\left[\frac{\omega_-}{\omega_i}\cos(\boldsymbol{k}_- \cdot \boldsymbol{r} - \omega_- t) + \frac{\omega_+}{\omega_i}\cos(\boldsymbol{k}_+ \cdot \boldsymbol{r} - \omega_+ t)\right] \tag{10}$$

and

$$D_\pm E_{\pm 2} = -\frac{2\pi e^2}{m_0}\alpha_i\epsilon_i \delta n_2\left[\frac{\omega_-}{\omega_i}\cos(\boldsymbol{k}_- \cdot \boldsymbol{r} - \omega_- t + \delta_i - \delta_e) + \frac{\omega_+}{\omega_i}\cos(\boldsymbol{k}_+ \cdot \boldsymbol{r} - \omega_+ t + \delta_i + \delta_e)\right], \tag{11}$$

and

$$D_\pm E_{\pm 3} = 0\,, \tag{12}$$

where $E_{\pm 1} = \epsilon_\pm \cos(\phi_\pm)\cos(\boldsymbol{k}_\pm \cdot \boldsymbol{r} - \omega_\pm t)$, $E_{\pm 2} = \alpha_\pm \epsilon_\pm \cos(\boldsymbol{k}_\pm \cdot \boldsymbol{r} - \omega_\pm t + \delta_\pm)$, $E_{\pm 3} = -\epsilon_\pm \sin(\phi_\pm)\cos(\boldsymbol{k}_\pm \cdot \boldsymbol{r} - \omega_\pm t)$, $\omega_\pm = \omega_i \pm \omega$, $\boldsymbol{k}_\pm = \boldsymbol{k}_i \pm \boldsymbol{k}$ and $D_\pm = k_\pm^2 c^2 - \omega_\pm^2 + \omega_{pe}^2$. Here, $\omega_{pe} = (4\pi n_0 e^2/m_0)^{1/2}$ is the plasma frequency. Equation (12) restricts the value of $\phi_\pm$ to 0 or π for $\epsilon_\pm \neq 0$ and $D_\pm \neq 0$.

Expressions $D_\pm$ are the dispersion relations for the Stokes mode $(\boldsymbol{k}_-, \omega_-)$ and the anti-Stokes mode $(\boldsymbol{k}_+, \omega_+)$, when the following resonant conditions are satisfied

$$\begin{aligned} \omega_i - \omega &= \omega_-, \qquad \boldsymbol{k}_i - \boldsymbol{k} = \boldsymbol{k}_-\,, \\ \omega_i + \omega &= \omega_+, \qquad \boldsymbol{k}_i + \boldsymbol{k} = \boldsymbol{k}_+\,. \end{aligned} \tag{13}$$

Multiplying equation (10) on both sides by $\cos(\boldsymbol{k}_i \cdot \boldsymbol{r} - \omega_i t)$ and neglecting the terms containing $(2\boldsymbol{k}_i, 2\omega_i)$ as being nonresonsnt, we get

$$D_\pm \epsilon_\pm \cos(\phi_\pm) = -\frac{4\pi e^2}{m_0}\epsilon_i \delta n_1\,. \tag{14}$$

Similarly, if we multiply equation (11) by $\cos(\boldsymbol{k}_i \cdot \boldsymbol{r} - \omega_i t + \delta_i)$, we obtain

$$D_\pm \alpha_\pm \epsilon_\pm \cos[\boldsymbol{k} \cdot \boldsymbol{r} - \omega t \pm (\delta_\pm - \delta_i)] = -\frac{4\pi e^2}{m_0}\alpha_i\epsilon_i \delta n_2 \cos(\boldsymbol{k} \cdot \boldsymbol{r} - \omega t + \delta_e)\,. \tag{15}$$

Similar to equations (13), it gives following conditions between the phases

$$\delta_\pm = \delta_i \pm \delta_e\,. \tag{16}$$

Dividing equation (15) by equation (14), we have

$$\alpha_\pm = \alpha_i \frac{\delta n_2}{\delta n_1}\cos(\phi_\pm) = \alpha_i R \cos(\phi_\pm)\,, \tag{17}$$

where $R = \delta n_2/\delta n_1$. The value of R is related to $\boldsymbol{E}_i$: δn_{e1} couples with $\boldsymbol{E}_{i1}$ and δn_{e2} couples with $\boldsymbol{E}_{i2}$. In the linear theory, it is not possible to determine R, but one expects that it may not differ too much from the value of α_i.

If we multiply equation (14) by ϵ_i and equation (15) by $\alpha_i\epsilon_i$ and subtract, we find

$$(\alpha_i\alpha_\pm - \cos\phi_\pm)\epsilon_\pm = \frac{4\pi e^2}{m_0}\epsilon_i(1 - \alpha_i^2 R)\frac{\delta n_1}{D_\pm}\,. \tag{18}$$

Now, we have to determine the electron density perturbations δn_1 and δn_2. Here, we neglect the ions' response because of their larger mass compared to that of the electrons. With the inclusion of the ponderomotive force, as a driving force, the Vlasov equation for the low-frequency response of electrons can then be written as

$$\frac{\partial f}{\partial t} + \boldsymbol{v} \cdot \nabla f + \frac{1}{m_0}(e\nabla\phi - \nabla\psi) \cdot \frac{\partial f}{\partial \boldsymbol{v}} = 0\,, \tag{19}$$

where $\phi(\boldsymbol{r}, t)$ is the scalar potential associated with the electrostatic waves, $f(\boldsymbol{r}, \boldsymbol{v}, t)$, is the particle distribution function and $\psi(\boldsymbol{r}, t)$ is

the ponderomotive potential. Linearizing equation (19) with $f(\boldsymbol{r}, \boldsymbol{v}, t) = f_0(\boldsymbol{v}) + \delta f_{e1}(\boldsymbol{r}, \boldsymbol{v}, t) + \delta f_{e2}(\boldsymbol{r}, \boldsymbol{v}, t)$, we get

$$\frac{\partial(\delta f_{e1})}{\partial t} + \frac{\partial(\delta f_{e2})}{\partial t} + \boldsymbol{v} \cdot \nabla(\delta f_{e1}) + \boldsymbol{v} \cdot \nabla(\delta f_{e2}) + \frac{1}{m_0}(e\nabla\phi - \nabla\psi) \cdot \frac{\partial f_0}{\partial \boldsymbol{v}} = 0 , \tag{20}$$

where $\delta f_{e1} = \delta f_1 \cos(\boldsymbol{k} \cdot \boldsymbol{r} - \omega t)$ and $\delta f_{e2} = \delta f_2 \cos(\boldsymbol{k} \cdot \boldsymbol{r} - \omega t + \delta_e)$. The ponderomotive force of the radiation field is given by $\boldsymbol{F}_\omega = -\nabla\psi$. It depends quadratically on the amplitude and leads to a slowly varying longitudinal field, corresponding physically to radiation pressure, which leads to slow longitudinal motions and modifies the density. The ponderomotive potential is given by

$$\psi = \frac{e^2}{2m_0}\left\langle \left(\mathrm{Re}\left| \frac{\boldsymbol{E}_i}{i\omega_i} + \frac{\boldsymbol{E}_-}{i\omega_-} + \frac{\boldsymbol{E}_+}{i\omega_+} \right| \right)^2 \right\rangle_\omega = \frac{e^2}{2m_0\omega_i^2}[\epsilon_i\epsilon_- \cos(\phi_-) \cos(\boldsymbol{k} \cdot \boldsymbol{r} - \omega t) + \alpha_i\alpha_-\epsilon_i\epsilon_- \cos(\boldsymbol{k} \cdot \boldsymbol{r} - \omega t + \delta_i - \delta_-)$$
$$+ \epsilon_i\epsilon_+ \cos(\phi_+) \cos(\boldsymbol{k} \cdot \boldsymbol{r} - \omega t) + \alpha_i\alpha_+\epsilon_i\epsilon_+ \cos(\boldsymbol{k} \cdot \boldsymbol{r} - \omega t + \delta_+ - \delta_i)] . \tag{21}$$

The angle brackets $\langle\ \rangle_\omega$ represent the ω frequency component of an average over the fast time scale ($\omega_i \gg \omega$).

To determine ϕ self-consistently we use Poisson equation, which gives

$$\phi = -\frac{4\pi e}{k^2}(\delta n_{e1} + \delta n_{e2}) . \tag{22}$$

Now, substituting the expressions for δf_{e1}, δf_{e2}, δn_{e1}, δn_{e2}, ϕ and ψ into equation (20), we have

$$\delta f_2 + \mu\,\delta f_1 + \frac{4\pi e^2}{m_0 k^2}\left\{\delta n_2 + \mu\,\delta n_1 + \frac{k^2}{8\pi m_0\omega_i^2}\left[\epsilon_i\epsilon_- \cos(\phi_-)\mu + \epsilon_i\epsilon_+ \cos(\phi_+)\mu \right.\right.$$
$$\left.\left. + \alpha_i\alpha_-\epsilon_i\epsilon_- \frac{\sin(\boldsymbol{k} \cdot \boldsymbol{r} - \omega t + \delta_i - \delta_-)}{\sin(\boldsymbol{k} \cdot \boldsymbol{r} - \omega t + \delta_e)} + \alpha_i\alpha_+\epsilon_i\epsilon_+ \frac{\sin(\boldsymbol{k} \cdot \boldsymbol{r} - \omega t + \delta_+ - \delta_i)}{\sin(\boldsymbol{k} \cdot \boldsymbol{r} - \omega t + \delta_e)}\right]\right\} \frac{\boldsymbol{k} \cdot (\partial f_0/\partial \boldsymbol{v})}{(\omega - \boldsymbol{k} \cdot \boldsymbol{v})} = 0 , \tag{23}$$

where $\mu = \sin(\boldsymbol{k} \cdot \boldsymbol{r} - \omega t)/\sin(\boldsymbol{k} \cdot \boldsymbol{r} - \omega t + \delta_e)$.

Equation (23) shows that $\delta_\pm = \delta_i \pm \delta_e$ and $\delta_e = 0$ or π. We obtain, for $\delta_e = \pi$,

$$\delta f_2 - \delta f_1 = -\frac{4\pi e^2}{m_0 k^2}\left(\delta n_2 - \delta n_1 + \frac{k^2}{8\pi m_0\omega_i^2} A\right)\frac{\boldsymbol{k} \cdot (\partial f_0/\partial \boldsymbol{v})}{(\omega - \boldsymbol{k} \cdot \boldsymbol{v})} , \tag{24}$$

where $A = (\alpha_i\alpha_- - \cos\phi_-)\epsilon_i\epsilon_- + (\alpha_i\alpha_+ - \cos\phi_+)\epsilon_i\epsilon_+$. The difference in the density perturbations $(\delta n_2 - \delta n_1)$ is given by

$$\delta n_2 - \delta n_1 = \int_{-\infty}^{\infty} n_0(\delta f_2 - \delta f_1)d\boldsymbol{v}$$
$$= -\left(\delta n_2 - \delta n_1 + \frac{k^2}{8\pi m_0\omega_i^2} A\right)\chi_e , \tag{25}$$

where

$$\chi_e = \frac{\omega_{pe}^2}{k^2}\int_{-\infty}^{\infty} \frac{\boldsymbol{k} \cdot (\partial f_0/\partial \boldsymbol{v})}{(\omega - \boldsymbol{k} \cdot \boldsymbol{v})} d\boldsymbol{v} , \tag{26}$$

is the electron susceptibility function (Liu & Kaw 1976; Fried & Conte 1961). Since $R = \delta n_2/\delta n_1$, from equation (25) we have

$$\left(1 + \frac{1}{\chi_e}\right)(1 - R)\delta n_1 = \frac{k^2}{8\pi m_0\omega_i^2} A . \tag{27}$$

Substituting equation (27) for δn_1 into equation (18), we obtain

$$\left(1 + \frac{1}{\chi_e}\right)(1 - R) = \frac{v_0^2 k^2}{2}\frac{(1 - R\alpha_i^2)}{(1 + \alpha_i^2)}\left(\frac{1}{D_-} + \frac{1}{D_+}\right) , \tag{28}$$

where $v_0 = [e\epsilon_i(1 + \alpha_i^2)^{1/2}/m_0\omega_i]$ is the quiver velocity of electrons in the field of incident EM wave. The energy density of the incident field and the luminosity L of the source are related by

$$\frac{1}{8\pi}\epsilon_i^2(1 + \alpha_i^2) = \frac{L}{4\pi r^2 c} , \tag{29}$$

where r is the distance between source of radiation and plasma. Therefore, the quiver velocity of electrons is given by

$$v_0 = \frac{e}{m_0}\left(\frac{2L}{r^2 c}\right)^{1/2}\frac{1}{\omega_i} . \tag{30}$$

Equation (28) is the plasma dispersion relation describing the SRS of elliptically polarized EM wave. The SRS instability resonantly

excites only when the frequency and wavenumber matching conditions (see eq. [13]) are satisfied. The simplest stimulated scattering process is the one involving only one high-frequency sideband, i.e., the Stokes component ($\boldsymbol{k}_-$, ω_-). Thus, we consider a case where $D_- \approx 0$ and $D_+ \neq 0$, i.e., the anti-Stokes component ($\boldsymbol{k}_+$, ω_+) is nonresonant. This approximation is justified as long as $\omega \ll (c^2\boldsymbol{k}_i \cdot \boldsymbol{k}/\omega_i)$; it breaks down for very small $\boldsymbol{k}$ (i.e., for long-wavelength electrostatic perturbations) or if $\boldsymbol{k}$ is nearly perpendicular to $\boldsymbol{k}_i$.

The value of k is approximately $2k_i$, corresponding to backward scattering ($\phi_- = \pi$) and for forward scattering ($\phi_- = 0$) it is approximately ω_{pe}/c. Thus, the growth rate of the instability attains its maximum value for backscatter. For the case of backscattering, $D_-(\boldsymbol{k}_-, \omega_-) \approx 2\omega_i(\omega - c^2\boldsymbol{k}_i \cdot \boldsymbol{k}/\omega_i + c^2k^2/2\omega_i) \approx 0$ for $\omega_i \gg \omega$. The dispersion relation for primarily backscatter is, therefore,

$$\left(1 + \frac{1}{\chi_e}\right)(1 - R) = \frac{1}{4}\frac{v_0^2 k^2}{\omega_i(\omega - \Delta)}\frac{(1 - R\alpha_i^2)}{(1 + \alpha_i^2)}, \tag{31}$$

where

$$\Delta = \boldsymbol{k} \cdot \boldsymbol{v}_g - \frac{k^2c^2}{2\omega_i} \tag{32}$$

with $\boldsymbol{v}_g = \boldsymbol{k}_i c^2/\omega_i$. From the equation (31), we can derive the threshold and the growth rate for the SRS instability. For $\omega^2 \approx \omega_e^2 = \omega_{pe}^2 + (3/2)k^2v_T^2$, the natural frequency of the plasma wave and $\omega_-^2 \approx \omega_{pe}^2 + c^2(\boldsymbol{k}_i - \boldsymbol{k})^2$, equation (31) can be written as

$$(\omega - \omega_e + i\Gamma_e)(\omega - \omega_e + i\Gamma_-)(1 - R) = -\frac{v_0^2 k^2 \omega_{pe}}{8\omega_i}\frac{(1 - R\alpha_i^2)}{(1 + \alpha_i^2)}, \tag{33}$$

where

$$\Gamma_e = \frac{\sqrt{\pi}}{2}\frac{\omega_{pe}}{(k\lambda_{De})^3}\exp\left[-\frac{1}{2(k\lambda_{De})^2} - \frac{3}{2}\right] + \nu_e \tag{34}$$

is the damping rate of the electron plasma wave, $\nu_e = 3.632 n_e \ln\Lambda/T_e^{3/2}$ is the electron collision frequency and Coulomb logarithm $\ln\Lambda \approx 10$. Here, $\Gamma_- = \omega_{pe}^2\nu_e/2\omega_-^2$ is the collisional damping rate of the scattered EM wave. Setting $\omega = \omega_e + i\Gamma$, and solving equation (33) for the growth rate Γ, we find

$$\Gamma = -\frac{1}{2}(\Gamma_e + \Gamma_-) \pm \frac{1}{2}\sqrt{(\Gamma_e - \Gamma_-)^2 + \frac{v_0^2 k^2 \omega_{pe}}{2\omega_i(1 + \alpha_i^2)}\frac{(1 - R\alpha_i^2)}{(1 - R)}}. \tag{35}$$

Setting $\Gamma = 0$, we obtain the threshold condition for the excitation of Raman scattering

$$\left(\frac{v_0}{c}\right)_{thr} = 2\frac{\Gamma_e\Gamma_-}{\omega_i\omega_{pe}}\frac{(1 + \alpha_i^2)(1 - R)}{(1 - R\alpha_i^2)}. \tag{36}$$

The growth rate just above the threshold is given by

$$\Gamma = \frac{v_0^2 k^2 \omega_{pe}}{8(\omega_i - \omega_{pe})\Gamma_e}\frac{(1 - R\alpha_i^2)}{(1 + \alpha_i^2)(1 - R)}, \tag{37}$$

which is proportional to E_i^2. The maximum growth rate attainable for $\omega_{pe} > \Gamma > \Gamma_e$, on the other hand, is

$$\Gamma = \frac{v_0 k}{2}\sqrt{\frac{\omega_{pe}}{2(\omega_i - \omega_{pe})}\frac{(1 - R\alpha_i^2)}{(1 + \alpha_i^2)(1 - R)}}. \tag{38}$$

For $k \approx 2k_i$, equation (38) becomes

$$\Gamma = \frac{e\epsilon_i}{m_0 c}\sqrt{\frac{\omega_{pe}}{2\omega_i}\frac{(1 - R\alpha_i^2)}{(1 - R)}}. \tag{39}$$

We note that backscatter by plasma wave is possible only if $2k_i\lambda_{De} \ll 1$. For $k_i\lambda_{De}$ not too small, the stimulated Compton backward scattering due to the nonlinear Landau damping of the beat mode by resonant electrons becomes important.

3. STOKES PARAMETERS

The polarization state of the incident radiation changes due to the stimulated Raman scattering in a plasma (see eqs. [1], [9], [16], with $\delta_e = 0$ or π). The Stokes parameters for the incident and scattered EM waves (Rybicki & Lightman 1979) are

$$I_j = \frac{c}{8\pi}(1 + \alpha_j^2)\epsilon_j^2, \tag{40}$$

$$Q_j = \frac{(1 - \alpha_j^2)}{(1 + \alpha_j^2)}I_j, \tag{41}$$

$$U_j = \frac{2\alpha_j}{(1 + \alpha_j^2)}I_j\cos(\delta_j), \tag{42}$$

and

$$V_j = -\frac{2\alpha_j}{(1+\alpha_j^2)} I_j \sin(\delta_j) . \tag{43}$$

The sense of rotation of the electric field is given by

$$\sin(2\beta_j) = \frac{V_j}{I_j} = -\frac{2\alpha_j}{(1+\alpha_j^2)} \sin(\delta_j) . \tag{44}$$

The magnitudes of the principle axes of the ellipse are

$$a_j = I_j|\cos(\beta_j)| \quad \text{and} \quad b_j = I_j|\sin(\beta_j)| . \tag{45}$$

The orientation of the major axis of the ellipse relative to the $\hat{e}_1$ axis is given by

$$\tan(2\chi_j) = \frac{U_j}{Q_j} = \frac{2\alpha_j}{(1-\alpha_j^2)} \cos(\delta_j) . \tag{46}$$

Here, $j = i$ for incident and $-$ for scattered EM waves.

We use the relations $\delta_e = \pi$, $\delta_- = \delta_i - \delta_e$ and $\alpha_- = \alpha_i R$ to compute the Stokes parameters for the scattered wave.

4. NUMERICAL SOLUTION OF EQUATION (28)

For a strongly damped electron plasma wave with $k_l \lambda_{De} \approx 0.4$, it is not possible to expand $\chi_e(\omega, k)$ in to an asymptotic series. The regime $k_l \lambda_{De} \approx 0.4$ corresponds to the transition region between SRS and stimulated Compton scattering (SCS) (Gangadhara & Krishan 1992). Therefore, using $\omega = \omega_e + i\Gamma$, we numerically solve equation (28) including all the damping effects.

4.1. *In Pulsars*

The typical values of the plasma and radiation parameters at a distance $r = 100\, R_{NS} = 10^8$ cm (neutron star radius $R_{NS} \approx 10$ km) in a pulsar are electron density $n_e = n_8 \times 10^8$ cm^{-3}, temperature $T_e = T_5 \times 10^5$ K, and luminosity $L = L_{30} \times 10^{30}$ ergs s^{-1} in the band $\Delta\nu < \nu = 600$ MHz (Gangadhara, Krishan, & Shukla 1993).

Figure 2 shows the e-folding time $t_e = 1/\Gamma$ as a function of ω_i/ω_{pe} at the different values of electron temperature T_e ($= 10^5$, 5×10^5, 10^6, and 7.5×10^6 K) for forward SRS of the incident wave. The frequency of the scattered EM wave is $\omega_- = \omega_i + \omega_e$. One recalls that at high temperatures an electron plasma wave experiences a small collisional damping but large Landau damping. The rather fast rise in t_e is obtained in the SCS regime ($k_e \lambda_{De} \geq 0.4$). The points indicated by C correspond to $k_e \lambda_{De} \approx 0.4$ and represent the change of scattering process from Raman to Compton.

We know from the observations of pulsar PSR 1133+16 by Cordes (1983) that flux $I_i = 10^{-20}$ ergs cm^{-2} s^{-1} Hz^{-1} at the radio frequency $\nu_i = 600$ MHz. To find the relation between the incident flux I_i and the scattered flux I_- we use condition for conservation of wave energy within the systems of waves, the Manley–Rowe relation (Weiland & Wilhelmsson 1977), given by

$$\frac{I_i}{\omega_i} = \frac{I_-}{\omega_-} . \tag{47}$$

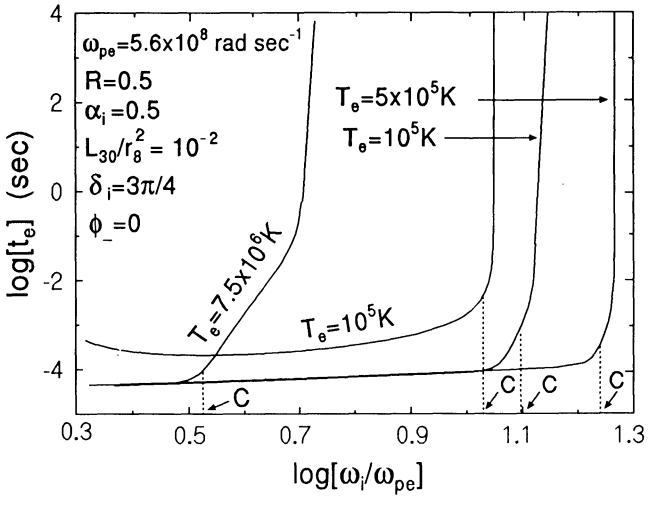

FIG. 2

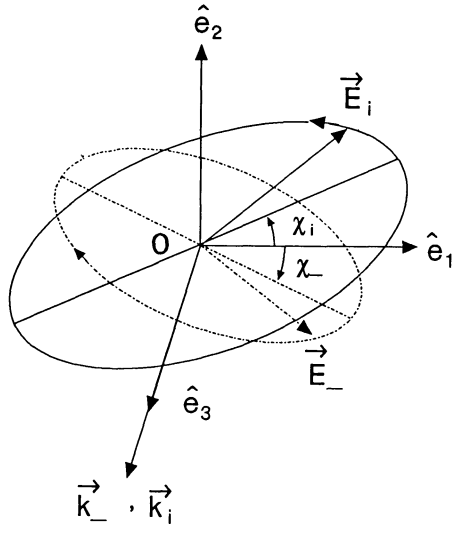

FIG. 3

FIG. 2.—The e-folding time $t_e = 1/\Gamma$ vs. the normalized frequency (ω_i/ω_{pe}). The points C represent the transition between SRS and SCS, where $k_l \lambda_{De} \approx 0.4$. At lower values of ($\omega_i/\omega_{pe}$), SRS occurs, while at higher values, SCS occurs.

FIG. 3.—The ellipses of the electric fields of the incident and forward-scattered EM waves

It gives

$$I_- = \left(1 - \frac{\omega}{\omega_i}\right) I_i \,. \tag{48}$$

For $\omega \approx \omega_{pe}$ and $\omega_i = 2.5\omega_{pe}$, we get $I_- = 0.6I_i$.

The sense of rotation and the orientation of the ellipses of the incident and the forward-scattered EM waves are shown in Figure 3.

In Table 1, the values of Stokes parameters for the incident and the forward-scattered EM waves in a pulsar PSR 1133+16 are listed. It shows that (1) a linearly polarized incident EM wave ($\delta_i = \pi$, $\alpha_i = 0.5$) scatters into another linearly polarized EM wave with its plane of polarization rotated through an angle χ_- with respect to $\hat{e}_1$ axis (see Fig. 3); (2) an elliptically polarized incident wave with counterclockwise sense ($\delta_i = 3\pi/4$, $\alpha_i = 1$) scatters into (*i*) a linearly polarized wave when $R = 0$, (*ii*) an elliptically polarized wave with clockwise sense and major axis rotated through an angle χ_- when $R = 0.4$, 0.8, and 1.2; (3) a circularly polarized incident wave with counterclockwise sense ($\delta_i = \pi/2$, $\alpha_i = 1$) scatters into (*i*) linearly polarized wave when $R = 0$, (*ii*) an elliptically polarized waves with clockwise sense when $R = 0.4$ and 0.8, (*iii*) circularly polarized wave with clockwise sense when $R = 1$.

TABLE 1

STOKES PARAMETERS OF THE INCIDENT AND FORWARD-SCATTERED EM WAVES FOR PSR 1133+16

A.

PARAMETERS (ergs cm^{-2} s^{-1} Hz^{-1})	INCIDENT WAVE: $\delta_i = \pi$, $\alpha_i = 0.5$	SCATTERED WAVE: $\delta_- = 0$			
		$R = 0$	$R = 0.4$	$R = 0.8$	$R = 1.2$
I	1.0000E−20	6.0000E−21	6.0000E−21	6.0000E−21	6.0000E−21
Q	6.0000E−21	6.0000E−21	5.5385E−21	4.3448E−21	2.8235E−21
U	−8.0000E−21	0.0	2.3077E−21	4.1379E−21	5.2941E−21
V	0.0	0.0	0.0	0.0	0.0
χ (rad)	−0.4636	0.0	0.1974	0.3805	0.5404
a	1.0000E−20	6.0000E−21	6.0000E−21	6.0000E−21	6.0000E−21
b	0.0	0.0	0.0	0.0	0.0
Sense of rotation	...	...	...	...	...
Nature	Linear	Linear	Linear	Linear	Linear

B.

PARAMETERS (ergs cm^{-2} s^{-1} Hz^{-1})	INCIDENT WAVE: $\delta_i = 3\pi/4$, $\alpha_i = 1$	SCATTERED WAVE: $\delta_- = -\pi/4$			
		$R = 0$	$R = 0.4$	$R = 0.8$	$R = 1.2$
I	1.0000E−20	6.0000E−21	6.0000E−21	6.0000E−21	6.0000E−21
Q	0.0	6.0000E−21	4.3448E−21	1.3171E−21	−1.0820E−21
U	−7.0711E−21	0.0	2.9260E−21	4.1392E−21	4.1731E−21
V	−7.0711E−21	0.0	2.9260E−21	4.1392E−21	4.1731E−21
χ (rad)	0.7853	0.0	0.2963	0.6314	−0.6586
a	9.239E−21	6.0000E−21	5.8064E−21	5.5705E−21	5.5618E−21
b	3.8268E−21	0.0	1.5118E−21	2.2291E−21	2.2510E−21
Sense of Rotation	Counterclockwise	...	Clockwise	Clockwise	Clockwise
Nature	Elliptical	Linear	Elliptical	Elliptical	Elliptical

C.

PARAMETERS (ergs cm^{-2} s^{-1} Hz^{-1})	INCIDENT WAVE: $\delta_i = \pi/2$, $\alpha_i = 1$	SCATTERED WAVE: $\delta_- = -\pi/2$			
		$R = 0$	$R = 0.4$	$R = 0.8$	$R = 1$
I	1.0000E−20	6.0000E−21	6.0000E−21	6.0000E−21	6.0000E−21
Q	0.0	6.0000E−21	4.3448E−21	1.3171E−21	0.0
U	0.0	0.0	0.0	0.0	0.0
V	−1.0000E−20	0.0	4.1379E−21	5.8536E−21	6.0000E−21
χ (rad)	...	0.0	2.9170E−17	1.3613E−16	...
a	7.0711E−21	6.0000E−21	5.5709E−21	4.6852E−21	4.2426E−21
b	7.0711E−21	0.0	2.2283E−21	3.7482E−21	4.2426E−21
Sense of Rotation	Counterclockwise	...	Clockwise	Clockwise	Clockwise
Nature	Circular	Linear	Elliptical	Elliptical	Circular

Similar to Table 1, the Stokes parameters of the incident and backward-scattered EM waves in PSR 1133+16 are listed in Table 2. In the case of backward SRS, sense reversal does not occur.

Figure 4 shows χ_- as a function of the e-folding time t_e, for different values of α_i in the case of forward scattering of the ellipticity polarized radio wave E_i, in the emission region of a pulsar. Here, R is varied between 0 and 1. For R close to 1, one observes $t_e \leq 10^{-4}$ s. The rotational angle χ_- reaches a maximum when the growth rate attains its maximum. It is seen that a reversal in the sense of polarization can take place in a time scale lying between micro- and milliseconds.

4.2. *In Quasars*

The typical values of the plasma and radiation parameters in the broadline region, at a distance $r = r_{pc} \times 3.086 \times 10^{18}$ cm from the central engine of a quasar, are (Krishan & Wiita 1990; Gangadhara & Krishan 1990) electron density $n_e = n_9 \times 10^9$ cm^{-3}, temperature $T_e = T_5 \times 10^5$ K, and luminosity $L = L_{42} \times 10^{42}$ ergs s^{-1} in the radio band $\Delta\omega \approx \omega_{pe}$.

Figure 5 shows χ_- as a function of the e-folding time t_e, for different values of α_i for forward scattering of the elliptically polarized

TABLE 2

STOKES PARAMETERS OF THE INCIDENT AND BACKWARD-SCATTERED EM WAVES FOR PSR 1133+16

A.

PARAMETERS (ergs cm^{-2} s^{-1} Hz^{-1})	INCIDENT WAVE: $\delta_i = \pi$, $\alpha_i = 0.5$	SCATTERED WAVE: $\delta_- = 0$			
		$R = 0$	$R = 0.4$	$R = 0.8$	$R = 1.2$
I	1.0000E−20	6.0000E−21	6.0000E−21	6.0000E−21	6.0000E−21
Q	6.0000E−21	6.0000E−21	5.5385E−21	4.3448E−21	2.8235E−21
U	−8.0000E−21	0.0	−2.3077E−21	−4.1379E−21	−5.2941E−21
V	0.0	0.0	0.0	0.0	0.0
χ (rad)	−0.4636	0.0	−0.1974	−0.38051	−0.54042
a	1.0000E−20	6.0000E−21	6.0000E−21	6.0000E−21	6.0000E−21
b	0.0	0.0	0.0	0.0	0.0
Sense of Rotation	...	...	...	...	...
Nature	Linear	Linear	Linear	Linear	Linear

B.

PARAMETERS (ergs cm^{-2} s^{-1} Hz^{-1})	INCIDENT WAVE: $\delta_i = 3\pi/4$, $\alpha_i = 1$	SCATTERED WAVE: $\delta_- = -\pi/4$			
		$R = 0$	$R = 0.4$	$R = 0.8$	$R = 1.2$
I	1.0000E−20	6.0000E−21	6.0000E−21	6.0000E−21	6.0000E−21
Q	0.0	6.0000E−21	4.3448E−21	1.3171E−21	−1.0820E−21
U	−7.0711E−21	0.0	−2.9260E−21	−4.1392E−21	−4.1731E−21
V	−7.0711E−21	0.0	−2.9260E−21	−4.1392E−21	−4.1731E−21
χ (rad)	−0.7854	0.0	−0.2963	−0.6314	0.6586
a	9.2388E−21	6.0000E−21	5.8064E−21	5.5705E−21	5.5618E−21
b	3.8268E−21	0.0	1.5118E−21	2.2291E−21	2.2510E−21
Sense of Rotation	Counterclockwise	...	Counterclockwise	Counterclockwise	Counterclockwise
Nature	Elliptical	Linear	Elliptical	Elliptical	Elliptical

C.

PARAMETERS (ergs cm^{-2} s^{-1} Hz^{-1})	INCIDENT WAVE: $\delta_i = \pi/2$, $\alpha_i = 1$	SCATTERED WAVE: $\delta_- = -\pi/2$			
		$R = 0$	$R = 0.4$	$R = 0.8$	$R = 1$
I	1.0000E−20	6.0000E−21	6.0000E−21	6.0000E−21	6.0000E−21
Q	0.0	6.0000E−21	4.3448E−21	1.3171E−21	0.0
U	0.0	0.0	0.0	0.0	0.0
V	−1.0000E−20	0.0	−4.1379E−21	−5.8537E−21	−6.0000E−21
χ (rad)	...	0.0	−2.9170E−17	−1.3612E−16	...
a	7.0711E−21	6.0000E−21	5.5709E−21	4.6852E−21	4.2426E−21
b	7.0711E−21	0.0	2.2283E−21	3.7482E−21	4.2426E−21
Sense of Rotation	Counterclockwise	...	Counterclockwise	Counterclockwise	Counterclockwise
Nature	Circular	Linear	Elliptical	Elliptical	Circular

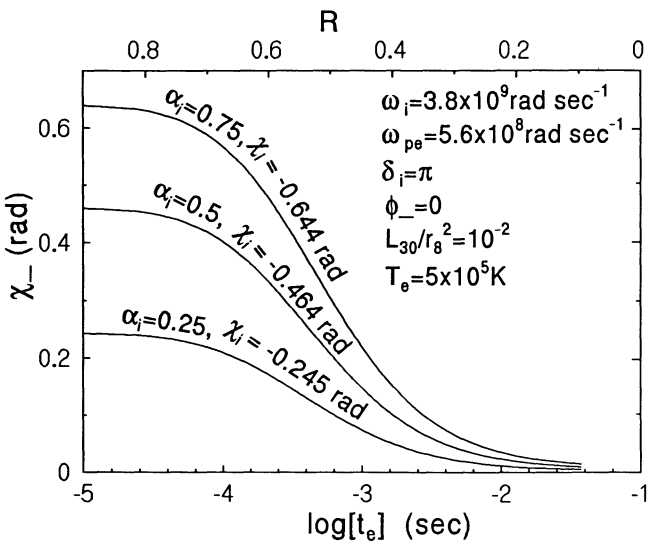

FIG. 4

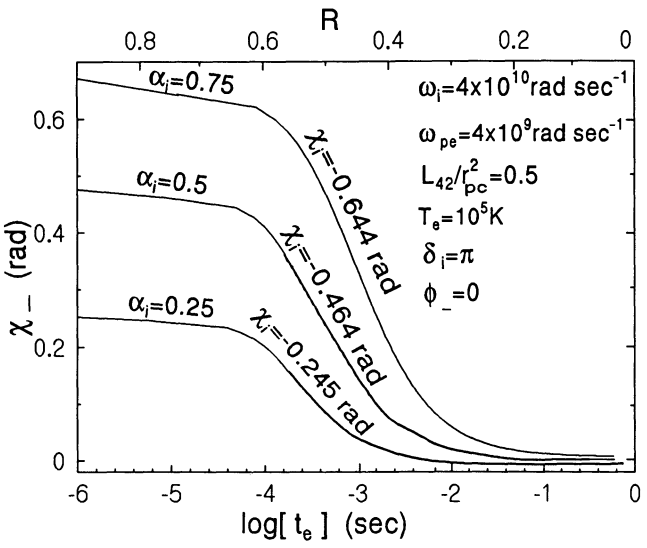

FIG. 5

FIG. 4.—The orientation angle χ_- of the scattered radiation vs. the e-folding time t_e for the SRS scattering of radio wave in a pulsar
FIG. 5.—The orientation angle χ_- of the scattered radiation vs. the e-folding time t_e for the SRS scattering of a radio wave in a quasar

radio wave $\boldsymbol{E}_i$ in a quasar. The rotational angle χ_- reaches a maximum when the growth rate attains its maximum. Similarly, Figure 6 shows χ_- as a function of the e-folding time t_e, at different values of α_i for forward scattering of the elliptically polarized optical wave $\boldsymbol{E}_i$ in a quasar.

We know from the multifrequency observations of 3C 273 by Courvoisier et al. (1987) that $I_i = 4.2266 \times 10^{-22}$ ergs cm^{-2} s^{-1} Hz^{-1} at the radio frequency $\nu_i = 6.366 \times 10^9$ Hz. For $\omega \approx \omega_{pe}$ and $\omega_i = 2.5\omega_{pe}$, we obtain from equation (48) that $I_- = 2.5360 \times 10^{-22}$ ergs cm^{-2} s^{-1} Hz^{-1}.

Similar to Table 1, in Table 3 the values of Stokes parameters for the incident and the forward-scattered EM waves in a quasar 3C 273 are listed. It has been observed that the variability in polarization of nonthermal radiation varies over the time scales ranging between one second and one day.

5. FARADAY ROTATION VERSUS STIMULATED RAMAN SCATTERING

Here, we make a comparison between the rotations of the plane of polarization produced by Faraday rotation and forward SRS, using the typical plasma and radiation parameters for a quasar. A linearly polarized EM wave which is incident on a plasma will be Faraday rotated through Ω_F rad, where Ω_F is given by (Lang 1974)

$$\Omega_F = \frac{2.36 \times 10^4}{\nu^2} \int_0^L n_e H \cos(\theta) dl \text{ rad}, \tag{49}$$

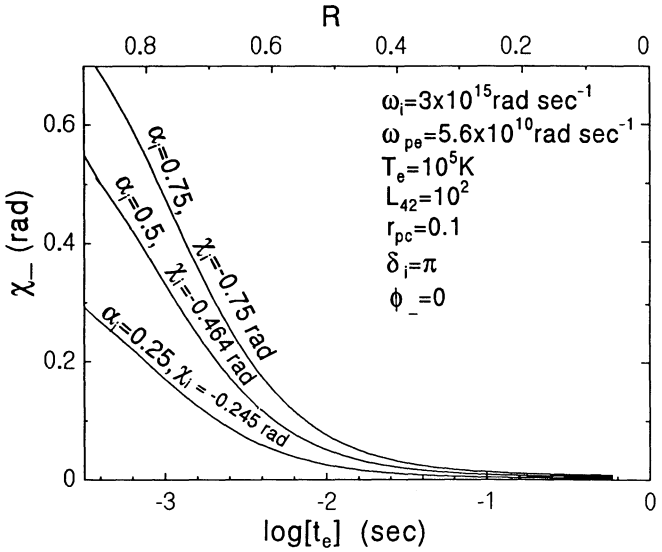

FIG. 6.—The orientation angle χ_- of the scattered radiation vs. the e-folding time t_e for the SRS scattering of optical wave in a quasar

TABLE 3

STOKES PARAMETERS OF THE INCIDENT AND FORWARD-SCATTERED EM WAVES FOR 3C 273

A.

PARAMETERS (ergs cm^{-2} s^{-1} Hz^{-1})	INCIDENT WAVE: $\delta_i = \pi$, $\alpha_i = 0.5$	SCATTERED WAVE: $\delta_- = 0$			
		$R = 0$	$R = 0.4$	$R = 0.8$	$R = 1.2$
I	4.2266E−22	2.5360E−22	2.5360E−22	2.5360E−22	2.5360E−22
Q	2.5360E−22	2.5360E−22	2.3410E−22	1.8364E−22	1.1934E−22
U	−3.3813E−22	0.0	9.7537E−23	1.7490E−22	2.2376E−22
V	0.0	0.0	0.0	0.0	0.0
χ (rad)	−0.4636	0.0	0.1974	0.3805	0.5404
a	4.2266E−22	2.5360E−22	2.5360E−22	2.5360E−22	2.5360E−22
b	0.0	0.0	0.0	0.0	0.0
Sense of Rotation	...	...	...	...	...
Nature	Linear	Linear	Linear	Linear	Linear

B.

PARAMETERS (ergs cm^{-2} s^{-1} Hz^{-1})	INCIDENT WAVE: $\delta_i = 3\pi/4$, $\alpha_i = 1$	SCATTERED WAVE: $\delta_- = -\pi/4$			
		$R = 0$	$R = 0.4$	$R = 0.8$	$R = 1.2$
I	4.2266E−22	2.5360E−22	2.5360E−22	2.5360E−22	2.5360E−22
Q	0.0	2.5360E−22	1.8364E−22	5.5667E−23	−4.5730E−23
U	−2.9887E−22	0.0	1.2367E−22	1.7495E−22	1.7640E−22
V	−2.9887E−22	0.0	1.2367E−22	1.7495E−22	1.7638E−22
χ (rad)	−0.7854	0.0	0.2963	0.6314	−0.6586
a	3.9049E−22	2.5360E−22	2.4541E−22	2.3544E−22	2.3507E−22
b	1.6174E−22	0.0	6.3896E−23	9.4217E−23	9.5139E−23
Sense of Rotation	Counterclockwise	...	Clockwise	Clockwise	Clockwise
Nature	Elliptical	Linear	Elliptical	Elliptical	Elliptical

C.

PARAMETERS (ergs cm^{-2} s^{-1} Hz^{-1})	INCIDENT WAVE: $\delta_i = \pi/2$, $\alpha_i = 1$	SCATTERED WAVE: $\delta_- = -\pi/2$			
		$R = 0$	$R = 0.4$	$R = 0.8$	$R = 1$
I	4.2266E−22	2.5360E−22	2.5360E−22	2.5360E−22	2.5360E−22
Q	0.0	2.5359E−22	1.8364E−22	5.5667E−23	0.0
U	0.0	0.0	0.0	0.0	0.0
V	−4.2266E−22	0.0	1.7489E−22	2.47410E−22	2.5360E−22
χ (rad)	...	0.0	2.9170E−17	1.3612E−16	...
a	2.9886E−22	2.5359E−22	2.3545E−22	1.9802E−22	1.7932E−22
b	2.9886E−22	0.0	9.4183E−23	1.5842E−22	1.7932E−22
Sense of Rotation	Counterclockwise	...	Clockwise	Clockwise	Clockwise
Nature	Circular	Linear	Elliptical	Elliptical	Circular

after traversing a thickness, L, of the plasma. Here, H is the magnetic field and θ is the angle between the line-of-sight and the direction of the magnetic field. For $n_e = n_9 \times 10^9$ cm^{-3}, $H = H_{-3} \times 10^{-3}$ G, and $\nu = \nu_9 \times 10^9$ Hz in the broad-line region of the quasar, we get

$$\Omega_F = 2.36 \times 10^{-8} \frac{n_9 H_{-3} L}{\nu_9^2} \text{ rad} . \quad (50)$$

Consider the point $\log (t_e) = -5$ s and $\chi_- = 0.65$ rad in Figure 5 on a curve with $\alpha_i = 0.75$ and $\chi_i = -0.644$ rad. The angle through which plane of polarization rotated due to SRS is given by $\Omega_{SRS} = \chi_- - \chi_i = 1.294$ rad during the time $t_e = 10^{-5}$ s. To compare Ω_F and Ω_{SRS} we need to convert t_e into the light travel distance $L = ct_e = 3 \times 10^5$ cm. Now, for $n_9 = 5$, $H_{-3} = 1$, and $\nu_9 = 6.366$ (Fig. 5), we get $\Omega_F = 8.735 \times 10^{-4}$ rad much smaller than Ω_{SRS}.

6. LARGE-AMPLITUDE EM WAVES AND THE EFFECT OF THEIR INCOHERENCE ON SRS INSTABILITY

The above results have been derived assuming the incident field to be monochromatic. In reality, however, some amount of incoherence is always present. It has been shown by Tamour (1973) and Thomson et al. (1974) that the effect of finite bandwidth $\Delta\omega_i$ of the incident field on the instability can be taken care of by replacing the damping rate of the sidebands Γ_L by $(\Gamma_L + 2\xi) \approx (\Gamma_L + \Delta\omega_i)$, where ξ is the number of phase jumps per unit time. This happens because Γ_L is a measure of the duration of time an electron is allowed to oscillate with the driving field before being knocked out of phase by a collision. The same effect results when the driving field suffers a phase shift and the two effects are additive. Thus replacing Γ_L by $\Gamma_L + \Delta\omega_i$ certainly raises the threshold for the instability.

If Γ is the growth rate due to a monochromatic pump at ω_i, then the actual growth rate Γ' due to the broad pump with a spectral width $\Delta\omega_i \gg \Gamma$ is given by (Kruer 1988)

$$\Gamma' = \frac{1}{\Delta\omega_i}\,\Gamma^2 . \tag{51}$$

Thus, the reduction in the growth rate due to the finite bandwidth may be compensated to some extent by the large luminosity radiation believed to be generated by coherent emission processes. Hence, the presence of incoherence through finite bandwidth in the radiation field effectively increases the damping rates and the thresholds and therefore reduces the growth rate (t_e increases) of SRS instability.

Several coherent processes such as (*i*) emission from bunches of relativistic electron beams (Ruderman & Sutherland 1975); (*ii*) curvature radiation (Gil & Snakowski 1990*a*, *b*; Asséo, Pellat, & Sol 1980), and (*iii*) parallel acceleration mechanism (Melrose 1978) have been proposed for the radio emission from pulsars. On the other hand, the role of the coherent emission processes for the generation of continuum emission of the quasar was emphasized long ago (Burbidge & Burbidge 1967) and has now begun to receive the attention it deserves (Lesch & Pohl 1992; Krishan & Wiita 1990; Weatherall & Benford 1991; Baker et al. 1988; Gangadhara & Krishan 1992).

Baker et al. (1988) constructed a model of the inner portions of astrophysical jets, in which a relativistic electron beam is injected from the central engine into the jet plasma. This beam drives electrostatic plasma wave turbulence, which leads to the collective emission of EM waves. Weatherall & Benford (1991) describe the scattering of charged particles from an intense localized electrostatic fields (cavitons) associated with plasma turbulence. These cavitons arise from a process known as plasma collapse (Zakharov 1972), in which electrostatic energy accumulates in localized wave packets. When the beam is ultrarelativistic, the emitted radiation is enhanced by relativistic beaming along the direction of propagation. In the same spirit, in this paper, we have studied the scattering of coherent EM radiation by electron density fluctuations or Langmuir waves of different phases in order to explain the polarization changes.

Analysis of the data by University of Michigan (Aller, Aller, & Hughes 1991) in the centimeter-wavelength regime showed both flux and linear polarization variability, and in addition polarization frequently exhibited position angle swings and large changes in percentage of polarization. To explain these observational results, one incorporates shock models with special geometries. While SRS, without invoking many constraints, can explain these results.

Sillanpää, Nilsson, & Takalo (1991) observed rotation of polarization position angle linearly 55° in 5 hr, in all five colors, in the optical regime. This is the fastest position angle swing ever observed at optical regions in OJ 287 or a blazar. It is difficult to explain this observed position angle swing with shocks in a jet model.

7. CONCLUSION

Usually, when one talks about polarization change, one is referring to the same wave. SRS, however, brings about change of frequency but when the frequency of the incident wave is much higher than the plasma frequency, the scattered wave frequency differs very little from the incident wave frequency.

The value of R can be determined only by the nonlinear calculations. However, one can easily expect that the value of R may be close to the value of α_i.

Similar to the frequency and wavenumber matching conditions (see eq. [13]), we found conditions between the phases δ_i, $\delta_\pm$, and δ_e (see eq. [16]) in the process of three-wave interaction.

Through SRS, the clockwise-polarized radiation can change into counterclockwise-polarized radiation and vice versa. In addition, circularly polarized wave can change into a linearly polarized, a circularly polarized, or an elliptically polarized wave or vice versa, depending upon the value of R. The plane of polarization gets rotated through an angle $(\chi_- - \chi_i)$. Compared to the Faraday rotation, the SRS is a faster process.

A direct measurement of the growth rate cannot be done by a remote observer. The *e*-folding time represents a characteristic time during which a significant change in the degree of polarization, sense, and rotation of plane of polarization takes place. Therefore, the observed variability time should be of the order of or a few times the *e*-folding time.

The features like a large change in rotation of polarization plane, sense reversal, and extremely rapid temporal changes would help to explain many observations, for which the existing mechanisms prove to be inadequate. Because of the very strong dependence of rotation angle on plasma parameters via the growth rate, in an inhomogeneous plasma medium, the depolarization is a natural outcome. A strong magnetic field can also affect the process: we intend to study this in detail in later work. We believe that the plasma process such as the SRS may be a potential mechanism for the polarization variability in pulsars and quasars.

We are grateful to Professor Abhijit Sen of the Institute of Plasma Research for critical reading of the manuscript.

REFERENCES

Aller, M. F., Aller, H. D., & Hughes, P. A. 1991, in Extragalactic Radio Sources—From Beams to Jets, ed. J. Roland, H. Sol, & G. Pelletier (Cambridge: Cambridge Univ. Press), 167
Asséo, E., Pellat, R., & Sol, H. 1980, in IAU Symp. 95, Pulsars, ed. W. Sieber & R. Wielebinski (Dordrecht: Reidel), 111
Baker, D. N., Borovsky, J. E., Benford, G., & Eilek, J. A. 1988, ApJ, 326, 110
Beal, J. H. 1990, in Physical Processes in Hot Cosmic Plasmas, ed. W. Brinkmann et al. (Dordrecht: Kluwer), 341
Benford, G. 1992, ApJ, 391, L59
Blandford, R. D., & Königl, A. 1979, ApJ, 232, 34
Burbidge, G. R., & Burbidge, E. M. 1967, Quasi-Stellar Objects (San Francisco: Freeman)
Cordes, J. M. 1983, in Positron-Electron Pairs in Astrophysics, ed. M. L. Burns, A. K. Harding, & R. Ramaty (AIP Conf. Proc., 101) (New York: AIP), 98
Cotton, W. D., Gelzahler, B. J., Marcaide, J. M., Shapiro, I. I., & Sanroma, M. 1984, ApJ, 286, 503
Courvoisier, T. J.-L., et al. 1987, A&A, 176, 197
Drake, J. F., Kaw, P. K., Lee, Y. C., Schmidt, G., Liu, C. S., & Rosenbluth, M. N. 1974, Phys. Fluids, 17, 778
Fried, D., & Conte, S. D. 1961, The Plasma Dispersion Function (New York: Academic)
Gangadhara, R. T., & Krishan, V. 1990, J. Astrophys. Astron., 11, 515
———. 1992, MNRAS, 256, 111
Gangadhara, R. T., Krishan, V., & Shukla, P. K. 1993, MNRAS, 262, 151
Gil, J. A., & Snakowski, J. K. 1990a, A&A, 234, 237
———. 1990b, A&A, 234, 269
Hasegawa, A. 1978, Bell System Tech. J., 57, 3069
Krishan, V., & Gangadhara, R. T. 1992, in International Conference on Plasma Physics, ed. K. Bethe & G. Thomas (Innsbruck: European Physical Soc.), III, 1671
Krishan, V., & Wiita, P. J. 1990, MNRAS, 246, 597
Kruer, W. L. 1988, The Physics of Laser-Plasma Interactions (New York: Addison-Wesley), 70
Lang, K. R. 1974, Astrophysical Formulae (Berlin: Springer-Verlag), 57
Lesch, H., & Pohl, M. 1992, A&A, 254, 29
Liu, C. S., & Kaw, P. K. 1976, Adv. Plasma Phys., 6, 83
Manchester, R. N., & Taylor, J. H. 1977, Pulsars (San Francisco: W. H. Freeman), 49
Melrose, D. B. 1978, ApJ, 225, 557
Ruderman, M., & Sutherland, P. 1975, ApJ, 196, 51
Rybicki, G. B., & Lightman, A. P. 1979, Radiative Processes in Astrophysics (New York: Wiley-Interscience), 62
Sillanpää, A., Nilsson, K., & Takalo, L. O. 1991, in Extragalactic Radio Sources—From Beams to Jets, ed. J. Roland, H. Sol, & G. Pelletier (Cambridge: Cambridge Univ. Press), 174
Stockman, H. S. 1978, in Pittsburgh Conference on BL Lac Objects, ed. A. M. Wolfe (Pittsburgh: Univ. of Pittsburgh), 149
Tamour, S. 1973, Phys. Fluids, 16, 1169
Thomson, J. J., Kruer, W. L., Bodner, S. E., & DeGroot, J. 1974, Phys. Fluids, 17, 849
van der Laan, H. 1966, Nature, 211, 1131
Weatherall, J. C., & Benford, G. 1991, ApJ, 378, 543
Weiland, J., & Wilhelmsson, H. 1977, Coherent Non-Linear Interaction of Waves in Plasmas (New York: Pergamon), 60
Zakharov, V. E. 1972, Sov. Phys.—JETP, 35, 908